Bioactive Materials 42 (2024) 366–378

Contents lists available at ScienceDirect

Bioactive Materials

journal homepage: www.keaipublishing.com/en/journals/bioactive-materials

Engineering anti-thrombogenic and anti-infective catheters through a stepwise metal-catechol-(amine) surface engineering strategy

Siyuan Yue [a,b], Wentai Zhang [b], Qing Ma [b], Zhen Zhang [c,**], Jing Lu [d,***], Zhilu Yang [a,b,*]

[a] School of Materials Science and Engineering, Southwest Jiaotong University, Chengdu 610031, China
[b] Dongguan Key Laboratory of Smart Biomaterials and Regenerative Medicine, The Tenth Affiliated Hospital of Southern Medical University, Dongguan, Guangdong, 523059, China
[c] Department of Cardiology, The Affiliated Hospital of Southwest Jiaotong University, The Third People's Hospital of Chengdu, Cardiovascular Disease Research Institute of Chengdu, Chengdu, 610031, China
[d] Department of Anesthesiology, Sichuan Provincial People's Hospital, University of Electronic Science and Technology of China, Chengdu, Sichuan, 610072, China

ARTICLE INFO

Keywords:
Nitric oxide
Antibacterial peptide
Efficient integration
Anticoagulant
Anti-inflection

ABSTRACT

Thrombosis and infection are pivotal clinical complications associated with interventional blood-contacting devices, leading to significant morbidity and mortality. To address these issues, we present a stepwise metal-catechol-(amine) (MCA) surface engineering strategy that efficiently integrates therapeutic nitric oxide (NO) gas and antibacterial peptide (ABP) onto catheters, ensuring balanced anti-thrombotic and anti-infective properties. First, copper ions were controllably incorporated with norepinephrine and hexanediamine through a one-step molecular/ion co-assembly process, creating a NO-generating and amine-rich MCA surface coating. Subsequently, azide-polyethylene glycol 4-N-hydroxysuccinimidyl and dibenzylcyclooctyne modified ABP were sequentially immobilized on the surface via amide coupling and bioorthogonal click chemistry, ensuring the dense grafting of ABP while maintaining the catalytic efficacy for NO. This efficient integration of ABP and NO-generating ability on the catheter surface provides potent antibacterial properties and ability to resist adhesion and activation of platelets, thus synergistically preventing infection and thrombosis. We anticipate that this synergistic modification strategy will offer an effective solution for advancing surface engineering and enhancing the clinical performance of biomedical devices.

1. Introduction

Skin-penetrating blood-contacting devices, such as indwelling catheters and external circuits, are indispensable in modern clinical treatments, supporting procedures such as hemodialysis [1], drug delivery [2], nutritional support [3], and extracorporeal circulation [4]. Despite their critical role, these devices are prone to thrombosis [5] and infection [6], which can lead to device failure [7], increased mortality rates and elevated medical costs [8,9]. To mitigate these complications, antibiotics and anticoagulants are routinely used in clinical practice [10–12]. However, their long-term use can result in severe side effects, including antibiotic-resistant bacteria [13,14], uncontrollable bleeding [15], thrombocytopenia [16], allergic reactions [17], epidermal necrolysis [18], deep phlebitis [19], and catheter-related bloodstream infections [20]. Consequently, there is an urgent need for safe and reliable treatments with fewer side effects that reduce the systematic use of antibiotics and anticoagulants [21–24].

Recently, surface engineering technologies that provide devices with local anticoagulant and antibacterial properties have emerged as promising solutions [25]. However, current surface modification strategies still struggle to effectively address both thrombosis and infection. Remarkably, healthy natural vasculature can sustain exceptional anti-inflection and anticoagulant properties for decades [26]. This ability is closely related to its physiological activity [27] and

Peer review under responsibility of KeAi Communications Co., Ltd.
* Corresponding author. School of Materials Science and Engineering, Southwest Jiaotong University, Chengdu, 610031, China.
** Corresponding author.
*** Corresponding author.
E-mail addresses: zhangzhen@swjtu.edu.cn (Z. Zhang), lujingmz@med.uestc.edu.cn (J. Lu), zhiluyang1029@swjtu.edu.cn (Z. Yang).

https://doi.org/10.1016/j.bioactmat.2024.09.009
Received 9 August 2024; Received in revised form 4 September 2024; Accepted 4 September 2024

microenvironment [28]. Antibacterial peptides (ABPs), a crucial part of innate immunity, are abundant in plasma and play a vital role in combating microbial pathogens [29]. Unlike traditional antibiotics that target specific bacterial proteins, ABPs destroy bacteria by inducing microbial membrane permeation through transient pore formation and can inhibit macromolecular synthesis [30], providing broader antimicrobial effects and reducing the potential for microbial resistance [31,32]. In addition, endothelium cells (ECs) continuously release NO into the blood microenvironment, effectively suppressing platelet adhesion and activation through cyclic guanosine monophosphate (cGMP) dependent pathways [33–36]. Inspired by these mechanisms, the combined use of NO and ABPs is anticipated to be an effective strategy for preventing both thrombosis and infection. However, efficiently integrating NO and ABPs onto device surfaces remains challenging.

In this study, we developed a surface engineering strategy that efficiently integrates NO-generating function and ABPs onto catheters, mimicking the synergistic anti-inflection and anticoagulant properties of natural vasculature. Specifically, the highly efficient NO catalytic substance, copper ions (Cu^{2+}), was first incorporated with norepinephrine (NE) and hexanediamine (HD) through a simple molecular/ion self-assembly process, forming a robust MCA (Cu-NE/HD) coating (Fig. 1). This process allows for the tailored content of Cu to control NO

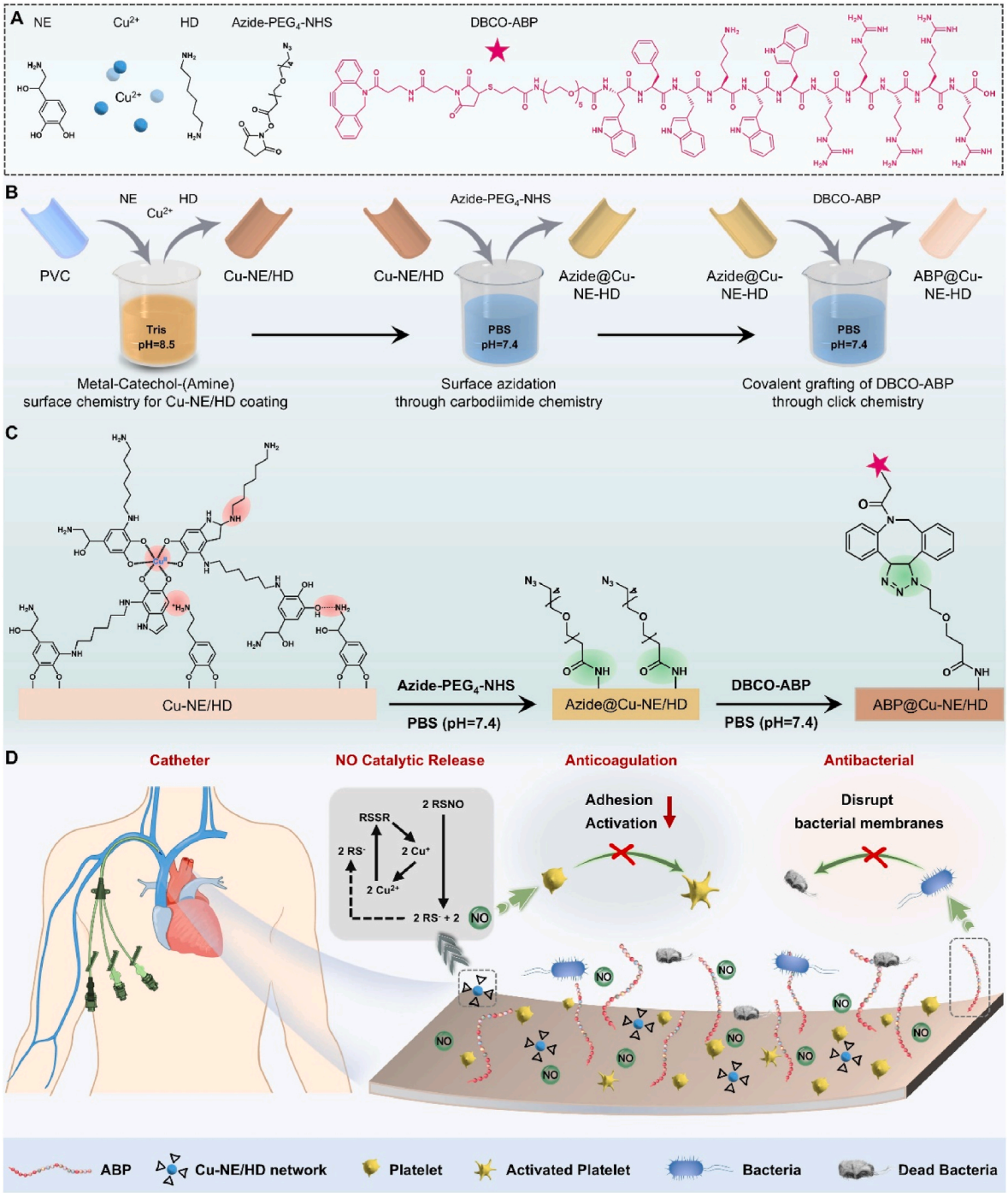

Fig. 1. (A) Reactants used for the fabrication of the coating. (B, C) Fabrication process involving a one-step molecular/ion co-assembly based on MCA chemical cross-linking, followed by the immobilization of Azide-PEG$_4$-NHS and DBCO-ABP through amide coupling and bioorthogonal click chemistry sequentially. (D) Synergistic regulation mechanism of NO and ABP for achieving anticoagulant and antibacterial properties.

generation, optimizing the anti-thrombosis properties. Then, the residual amine groups on the surface facilitated the sequential immobilization of azide-polyethylene glycol 4-N-hydroxysuccinimidyl (Azide-PEG_4-NHS) and dibenzylcyclooctyne modified ABP (DBCO-ABP) through amide coupling and bioorthogonal click chemistry [37,38]. This secondary grafting process not only ensures a high grafting density of ABP but also maintains the efficacy of NO catalytic generation. The engineered coating not only substantially improves resistance to thrombosis but also effectively inhibits bacterial adhesion and proliferation, showcasing the efficient integration and synergistic functionality of the dual-purpose design. These impressive outcomes provide new solutions for advancing the functionality of skin-penetrating blood-contacting devices.

2. Materials and methods

2.1. Materials

NE (purity ≥98.0 %), HD (purity ≥98.0 %), copper chloride dehydrate ($CuCl_2{\cdot}2H_2O$), N-(3-dimethylaminopropyl)-N′-ethylcarbodiimide (EDC, purity ≥98.0 %), N-hydroxysuccinimide (NHS, purity ≥97.0 %), 2-(N-morpholino) ethanesulfonic acid hydrate (MES, purity ≥97.0 %), NaOH (purity ≥98.0 %), Tris-HCl (purity ≥97.0 %), Acid Orange II (AO II), phosphate buffer solution (PBS), S-nitrosoglutathione (GSNO, purity ≥97.0 %), L-glutathione (GSH, purity ≥97.0 %), and Azide-PEG_4-NHS ester (purity ≥95.0 %) were purchased from Sigma-Aldrich (Shanghai, China). DBCO-ABP (purity ≥95.0 %) was prepared through the Fmoc-mediated solid-phase synthesis technique with assistance from China Peptides Co. Ltd. (Shanghai, China). Polyvinyl chloride (PVC) cardiopulmonary perfusion tubing was obtained from Changzhou LaiJie General Healthcare Material Co., Ltd (Changzhou, China).

2.2. Identification of DBCO-ABP

The molecular weight of DBCO-ABP was determined by Electrospray Ionization Mass Spectrometry (ESI-MS) using a PerkinElmer API 150EX LC/MS coupled with an Agilent 1100 HPLC system. The parameters were set as follows: buffer composition of 75 % ACN, 24.5 % H_2O and 0.5 % Ac, flow rate of 0.2 mL/min, and a run time of 1 min. The structural confirmation of DBCO-ABP was performed using a Bruker AVANCE III 400 MHz NMR spectrometer.

2.3. Preparation of ABP@Cu-NE/HD coatings

The Cu-NE/HD coating was fabricated on the PVC substrates via a one-step dip-coating process. Specifically, the substrates were immersed in a 10 mM Tris-HCl buffer (pH 8.5) containing 0.5 mg/mL NE, 2.106 mg/mL HD and 100 mg/mL $CuCl_2{\cdot}2H_2O$. The same fabrication procedure, but without the addition of $CuCl_2{\cdot}2H_2O$, was applied for the NE/HD coating. The immersion was conducted at 37 °C for 48h. Subsequently, the substrates were ultrasonically cleaned in distilled water to remove loosely bound reactants and dried.

For the grafting of ABP, the Cu-NE/HD and NE/HD modified substrates were first immersed in PBS (pH 8.0) containing 0.1 mg/mL Azide-PEG_4-NHS at room temperature for 12 h. After azidation, the substrates were incubated with 2 mg/mL DBCO-ABP at 4 °C for 12 h. Then, the ABP-coated substrates were washed with deionized water and dried under N_2 for further use.

2.4. Characterization

The density of amine groups was quantified using the Acid Orange II (AO II) colorimetric method. Samples were immersed in a 500 μmol/L AO-HCl solution (pH 3) for 7 h, followed by three washes with pH 3 HCl solution. Subsequently, the samples were placed in pH 12 NaOH solution and agitated for 30 min at room temperature to elute the surface bound AO. Finally, 150 μL of the desorbed AO supernatant was transferred to a 96-well plate, and the optical density was measured at 485 nm using a μQuant microplate reader (BioTek Instruments). The concentration of AO II indicated the amine concentration on the samples.

The grafting amount of Azide-PEG_4-NHS ester and DBCO-ABP were real-time monitored using a quartz crystal microbalance equipped with dissipation (QCM-D, Q-Sense AB, Sweden). Firstly, an AT-cut 5 MHz Au chip was modified with the Cu-NE/HD coating. The coated chip was then placed in the QCM-D chamber and PBS was introduced at a flow rate of 50 μL/min until the QCM traces stabilized. Subsequently, solutions of 0.1 mg/mL Azido-PEG_4-NHS and DBCO-ABP in PBS were pumped sequentially into the chamber. The frequency shifts (Δf) were recorded and converted into mass changes (Δm) using the Sauerbrey equation. Film thickness was determined using a spectroscopic ellipsometer (M − 2000V, J.A. Woollam, USA), with Δ and Ψ values recorded from 370 to 1000 nm and analyzed using the Cauchy model. Surface water contact angles (WCAs) were measured using a Krüss GmbH DSA 100 Mk 2 goniometer. Sessile drops of ultrapure water (2 μL) were deposited on various substrates at room temperature, and WCAs were determined using DSA 1.8 software. Each group included four samples, with three regions per sample tested. Chemical compositions of the coatings were analyzed using XPS (K-Alpha, Thermo Electron, USA) equipped with a monochromatic Al Kα source. The system operated at 12 kV and 15 mA under a pressure of 3×10^{-7} Pa, with charge calibration referenced to the graphitic carbon peak at 285 eV.

Chemical structures were analyzed using grazing angle attenuated total reflection Fourier transform infrared spectroscopy (GATR-FTIR, NICOLET 5700), matrix-assisted laser desorption/ionization mass spectrometry (MALDI-MS, Waters Micro MX, operating in reflection mode with a 337 nm N_2 laser), electron paramagnetic resonance (EPR, Bruker A320, Germany), and UV–visible spectroscopy (UV-1601, Shimadzu, Japan). For MALDI-MS analysis, a MALDI micro-MX time-of-flight mass spectrometer (Waters, Milford, MA) operating in reflection mode was employed. The MALDI source was equipped with a 337 nm N_2 laser operating with 4 ns-duration pulses, and the laser pulse energy was set at 200 arbitrary units (AU) when using 2, 5-dihydroxybenzoic acid (DHB) as the matrix. Mass spectra were collected in the range of 50–4000 *m/z*, averaging the ions generated from ten laser shots for each mass spectrum. A total of 10 mass spectra were collected for data analysis of each sample. Matrix solutions were prepared by dissolving DHB in 0.1 % TFA/acetonitrile (v/v, 1:4) at a final concentration of 20 mg/mL. In the case of MALDI analysis of Cu-NE/HD coating, stainless steel MALDI target plates were directly modified with the coating. Before analysis, 1 μL of the matrix solution was added to the polymeric-modified plates and allowed to air dry.

2.5. Cytotoxicity testing

ECs were obtained from Procell Life Science & Technology Co., Ltd. The cells were cultured in DMEM/F12 complete medium supplemented with 15 % Excell FBS and 1 % PS. Cells were seeded at a density of 1×10^4 cells/cm^2 on the sample surface and incubated at 37 °C with 5 % CO_2. After 72 h of incubation, cell viability was assessed using the cell counting kit-8 (CCK-8) assay to evaluate the cytocompatibility of the samples.

2.6. Catalytic generation of NO

A chemiluminescence NO analyzer (NOA, Seivers 280i, Boulder, CO) was employed to determine the real-time generation rate of NO. Briefly, the ABP@Cu-NE/HD-modified PVC substrates (5 mm × 10 mm) were immersed in PBS containing SNAP (10 μM) and GSH (10 μM). Then, the generated NO was conveyed into the NO analyzer by a stream of N_2 and the NO flux was calculated using a calibration line.

2.7. Antibacterial assays

The evaluation on antibacterial activities of the ABP@Cu-NE/HD coatings were conducted following the standard ISO22196-2011 [39]. Both gram-positive *Staphylococcus epidermidis* (*S. epidermidis*), strain American type culture collection (ATCC) 6538, and gram-negative *Escherichia coli* (*E. coli*), strain ATCC 25 922, were selected for the antimicrobial tests. Firstly, *S. epidermidis* and *E. coli* were precultured and diluted to a concentration of 6×10^5 cells/mL with nutrient broth. The samples were UV-sterilized and placed in sterile Petri dishes. Then, 0.1 mL of diluted bacterial solution was dropped onto the samples surfaces and covered with a polyethylene membrane (2.0 cm × 2.0 cm × 0.05 mm). The bacterial solution was spread to the edges, and the air bubble between the substrate surface and the membrane was gently expelled. Subsequently, all samples were incubated at 35 ± 1 °C and a humidity ≥90 % for 24 h. After incubation, the samples were gently removed and rinsed slowly with normal saline. Finally, the samples were inverted on agar and cultured under the aforementioned conditions for 24 h and observed by scanning electron microscopy (SEM) (ZEISS EVO 18). The antibacterial rate (R) was calculated using the following formula:

$$R = (Nc\text{-}N)/Nc \times 100\%$$

where Nc and N represent the numbers of the colonies on the control sample and the modified sample, respectively.

For further determining the antibacterial activity of the ABP@Cu-NE/HD coating a solution culture method was performed. Fresh bacterial colonies (1–2 colonies) from solid medium were transferred to liquid medium and incubated for 24 h. All samples were placed in a 24-well plate and incubated with 200 μL of the diluted bacterial solution (10^6 CFU/mL) at 37 °C. After 12 h, 800 μL of liquid medium was added to the wells and incubated for an additional 12 h. Finally, 200 μL of the solution was collected and the optical density (OD) at 600 nm was measured.

2.8. Platelet adhesion

For platelet adhesion and activation assays, platelet-rich plasma (PRP) was prepared by centrifugation of fresh rabbit blood at 1500 rpm for 15 min. Anticoagulation was achieved by adding trisodium citrate at a volume ratio of 9:1. Each sample was treated with 0.1 mL of PRP and incubated for 30 min at 37 °C. Subsequently, the samples underwent three washes with saline, and then were fixed with 2.5 % glutaraldehyde overnight. Then the samples were dehydrated using a gradient mixture of ethanol and water. Finally, SEM analysis was employed to assess both adhesion number and activation extent of platelets on the samples surfaces.

2.9. Bacterial infection assay in rat subcutaneous model

All the animal experiments were approved by the Dongguan People's Hospital Laboratory Animal Welfare and Ethics Committee (Approval NO: IACUC-AWEC-202306111), following the guidelines of the Laboratory Animal Administration Rules of China. Aseptic intravenous catheters (TPU, 24G) were sectioned into 1 cm slices. *S. epidermidis* and *E. coli* were diluted to the concentrations ranging from 5×10^5 to 1×10^6 CFU/mL using nutrient broth. The samples were then exposed to this bacterial solution for 8 h at 37 °C. Subsequently, the samples were collected and soaked in physiological saline at room temperature for approximately 2 h. Following this, the samples were implanted into subcutaneous pockets on the backs of Sprague-Dawley (SD) rats, and the incisions were sutured using surgical thread. Four SD rats were allocated for each bacterial strain, specifically *E. coli* and *S. epidermidis*. After 5 days of implantation, the rats were euthanized, and the implantation sites were examined for any significant changes. The samples were then retrieved for photographic documentation and hematoxylin and eosin (H&E) staining [40].

2.10. Anti thrombogenicity test by ex vivo blood circulation

Eight adult New Zealand white rabbits (2.5–3.5 kg) were selected for this experiment. All animals were administered general anesthesia prior to the experiments. The left carotid artery and the right jugular vein of each rabbit were surgically isolated and connected to an arteriovenous extracorporeal circulation system (ECC) using cannulas. Bare and modified PVC tubes were securely integrated into the ECC equipment. The blood circulation was maintained for 3 h through the ECC system. Post-circulation, the flow rates within the circuits were measured. Cross-sectional images of the tubes were captured, and the weight of any residual thrombus inside the tubes was recorded to evaluate the anticoagulant effectiveness of the coatings. Meanwhile, the tubes were fixed in 2.5 % glutaraldehyde solution overnight. After dehydration and critical point drying, the luminal surface of the tubes was observed by SEM.

2.11. Blood analysis by ex vivo blood circulation

To mimic clinical practice, a prolonged tubing (length 1.6 m) was employed in *ex vivo* blood circulation to maximize the contact area (~150 cm^2) between the tubing and the blood [41]. The whole blood was collected at 0, 5, 30, and 60 min during circulation for hematological and blood biochemistry analysis, including complete blood counts, activated partial thromboplastin time (APTT), and analysis of multiple serum indicators (CRP, IL-10, C3a, F_{1+2}, TNF-α, ALT, and CREA) using enzyme-linked immunosorbent assays (ELISAs).

All measurements for the analysis of indicators were conducted using ELISA and the routine blood and biochemical indexes were determined by the Chengdu Lilai Biotechnology Co., Ltd.

2.12. Long-term stability of the ABP@Cu-NE/HD coating

To assess the long-term antibacterial and antithrombotic properties of the ABP@Cu-NE/HD-coating, modified samples were immersed in PBS at 37 °C for 15 and 30 days. After immersion, the antibacterial and *ex vivo* anticoagulant performance of samples were evaluated as previously described.

2.13. Statistical analysis

All data are presented as mean with standard deviation unless otherwise indicated. All experiments were independently repeated at least three times, unless otherwise indicated. T-tests and one-way ANOVA were performed using GraphPad Prism 9.0 (GraphPad Software) for statistical analyses of different groups. Significance was denoted as follows: (ns: $p > 0.05$, *: $p \leq 0.05$, **: $p \leq 0.01$, ***: $p \leq 0.001$).

3. Results and discussion

3.1. Preparation of the ABP@Cu-NE/HD coating

Cu-NE/HD coatings were prepared with various concentrations of $CuCl_2{\cdot}2H_2O$ (0, 0.01, 0.05, 0.1, 0.5, and 1 mg/mL). As shown in Fig. 2A, the coatings exhibited a dark brown color with slight changes as Cu^{2+} concentration increased. At the same time, the hydrophilicity of all coatings was improved compared with bare PVC (Fig. S1). Furthermore, the thickness (Fig. 2B) of the coatings increased with higher Cu^{2+} concentration. However, it is worth noting that when the feeding concentration of $CuCl_2{\cdot}2H_2O$ exceeds 0.1 mg/mL, the thickness began to decline. This is mainly due to the enhanced coordination between Cu and phenolic hydroxyl groups of the NE molecule, which reduces the reaction sites between NE and HD molecule, thereby decreasing the formation efficacy of the coating [42,43]. To further investigate the

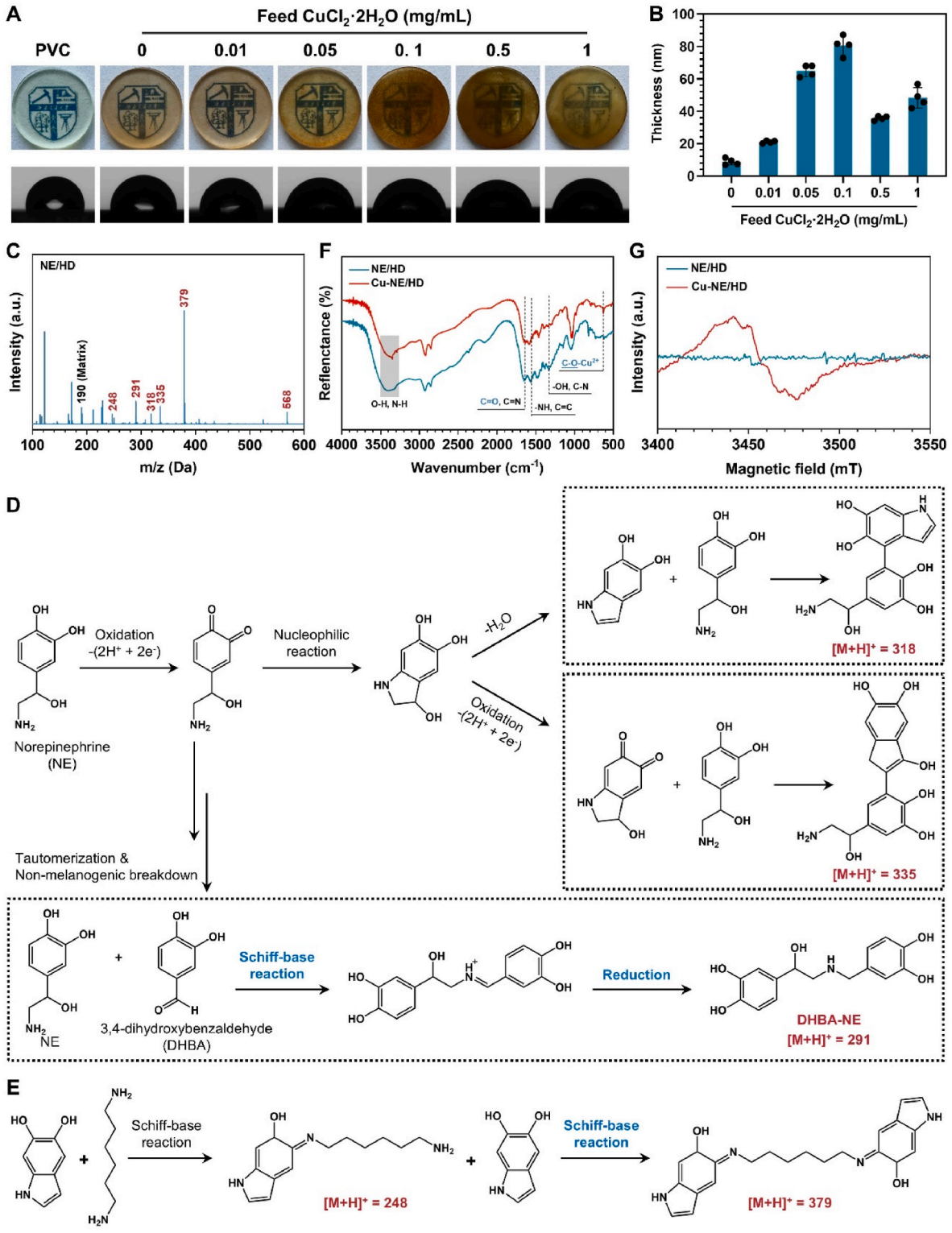

Fig. 2. (A) The photography and WCAs of the Cu-NE/HD coatings fabricated by $CuCl_2{\cdot}2H_2O$ with different feeding concentrations ranging from 0 to 1 mg/mL. (B) The thickness of the Cu-NE/HD coatings. (C) MALDI MS analysis of the NE/HD coating. (D) Suggested polymerization manner of NE and plausible structure of poly (norepinephrine) (pNE) based on MALDI MS analysis [26]. (E) Scheme of the possible mechanism of the NE/HD coating formation. (F) GATR-FTIR of the NE/HD and Cu-NE/HD coatings. (G) ESR spectrum of the NE/HD and Cu-NE/HD coatings.

formation mechanism of the coating, we utilized matrix-assisted laser desorption/ionization mass spectrometry (MALDI-MS), grazing angle attenuated total reflection Fourier transform infrared spectroscopy (GATR-FTIR) and electron paramagnetic resonance (EPR) analysis. As reported by Lee et al., in 2013 [44], the self-polymerization of NE involves the oxidation of NE to O-quinone, leading to the formation of intermediates such as 5,6-dihydroxyindole (DHI), 3-hydroxy-2,3-dihydro-1H-indole-5,6-dione (HDID), and 3,4-dihydroxybenzaldehyde (DHBA) through nucleophilic reactions, dehydration, reoxidation, tautomerization, and non-melanogenic degradation (Fig. 2D). These

intermediates subsequently undergo intermolecular reactions to form polymers. In our study, MALDI-MS analysis identified $[M+H]^+$ ion peaks at 291, 318, and 335 *m/z* corresponding to the reactions of NE with DHI, HDID, and DHBA (Fig. 2C). Additional peaks at 248 and 379 *m/z* indicate cross-linking between DHI and HD via Schiff-base reactions (Fig. 2E), and a peak at 568 *m/z* suggests cation-π interactions between the benzene ring of NE and $-NH_3^+$ groups from HD or NE (Fig. S2). Due to sample insolubility during MALDI-MS analysis of the Cu-NE/HD coating, we shifted to alternative analytical methods. GATR-FTIR analysis revealed a significant attenuation of the C=O stretching (quinone) peak at 1620 cm^{-1} and the emergence of a new Cu-O stretching vibration peak at 620 cm^{-1} for the Cu-NE/HD coating (Fig. 2F) [45]. This suggests that the coordination between catechol and copper ions inhibits further oxidation of the phenolic hydroxyl group to quinone. EPR characterization supported this, showing a signal range of 3490-3430 mT indicative of Cu^{2+}-NE coordination complexes (Fig. 2G). The formation of the coating is driven by Schiff-base reactions that facilitate cross-linking between NE and HD, alongside cation-π interactions between $-NH_3^+$ groups and the benzene ring. Copper ions are incorporated into the coating through coordination interactions with catechol.

The grafting of DBCO-ABP requires amine groups in the coating, which reached a maximum when the feeding concentration of $CuCl_2{\cdot}2H_2O$ exceeds 0.1 mg/mL (Fig. 3A). XPS analysis revealed a distinct Cu2p peak on the Cu-doped coatings (Fig. S3). Meanwhile, with the increase in $CuCl_2{\cdot}2H_2O$ feeding concentration, the content of element Cu in the coating also increased (Fig. 3B), indicating the tunability of Cu content in the coating. In our design, Cu^{2+} acts as a catalyst for the decomposition of endogenous S-nitrosothiols (RSNO) into NO. To determine the optimal Cu concentration for effective NO release, we evaluated the *in vitro* NO catalytic activity of PVC coated with different Cu levels. NO generation was monitored in a deoxygenated NO donor solution (pH 7.4) containing 10 μM GSNO and 10 μM reduced GSH using chemiluminescence. Real-time monitoring indicated that NO release rates were 3.1, 4.7, 5.8, 14.7 and 80.0 × 10^{-10} mol cm^{-2} min^{-1} for $CuCl_2{\cdot}2H_2O$ concentrations of 0, 0.01, 0.05, 0.1, 0.5, and 1 mg/mL, respectively (Fig. 3C and Fig. S4). Notably, NO release exceeded the physiological rate of 4 × 10^{-10} mol cm^{-2} min^{-1} when Cu concentration was higher than 0.05 mg/mL [46]. Further cytotoxicity testing showed no significant toxicity at various Cu concentrations in the absence of donors. However, the presence of donors revealed some cytotoxicity at $CuCl_2{\cdot}2H_2O$ concentrations of 0.5 and 1 mg/mL, attributed to the accumulation of excessive NO (Fig. 3D–F). To determine the optimal Cu-NE/HD coating for grafting antimicrobial peptides, we analyzed the surface amine groups, catalytic NO release rate, and endothelial toxicity using a heat map (Fig. 3G). The optimal coating was identified with a $CuCl_2{\cdot}2H_2O$ concentration of 0.1 mg/mL, which displayed abundant reactive functional groups, a sufficient NO release rate, and no cytotoxicity to ECs.

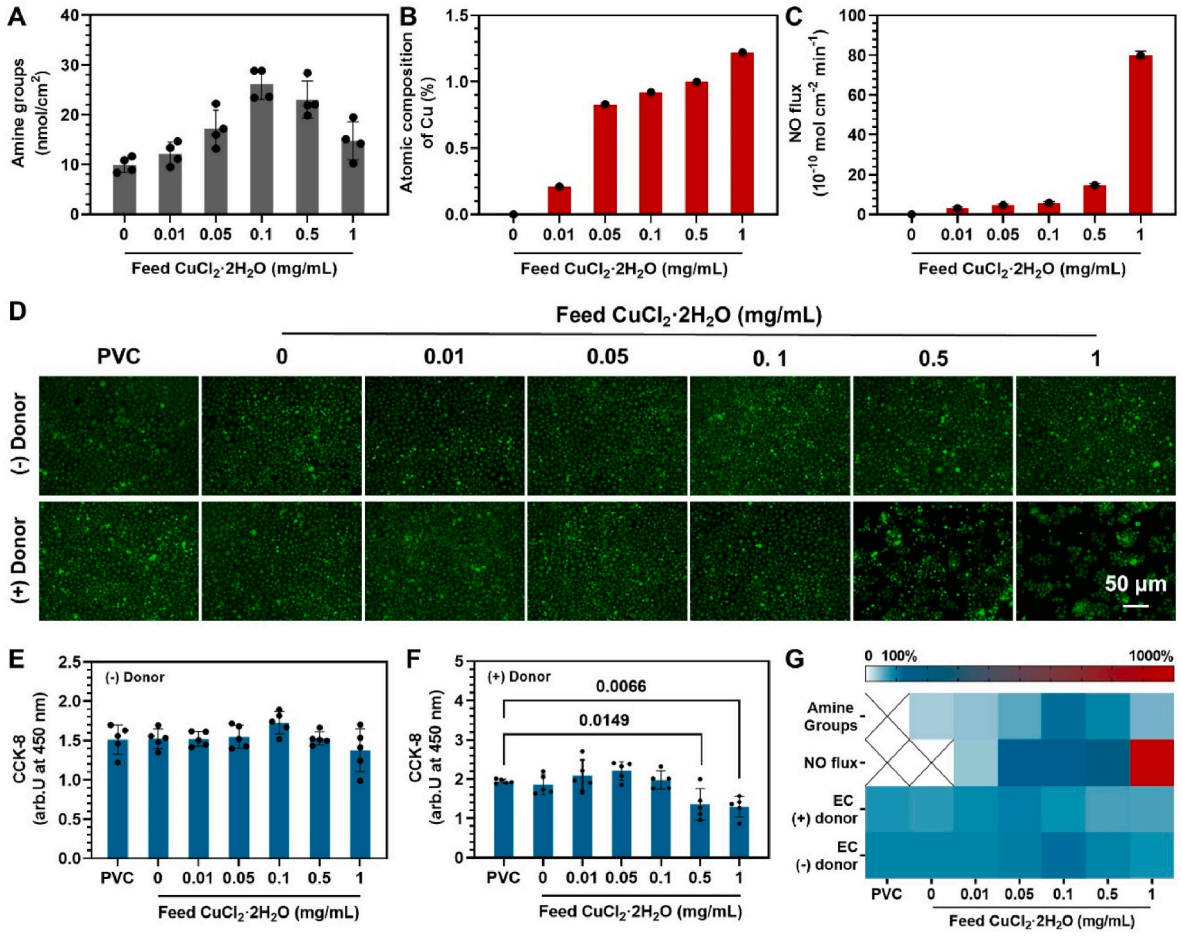

Fig. 3. (A) The surface amine groups of the Cu-NE/HD coatings. The contents of Cu (B) and NO release rates (C) of the Cu-NE/HD coatings. (D) Fluorescence staining of ECs cultured on PVC, and Cu-NE/HD coatings fabricated with different feeding concentrations of $CuCl_2{\cdot}2H_2O$ with or without NO donor (10 μM GSNO, 10 μM GSH) for 72 h. (E, F) Bioactivity of ECs on different surfaces, determined using CCK-8 assay. (G) Heat map of Cu-NE/HD coating-preferred properties in terms of the ability of secondary reaction immobilized biomolecules, regulation EC growth and NO release rates. Data are presented as mean ± SD ($n = 5$) and analyzed using a one-way ANOVA.

3.1.1. Characterization of the ABP@Cu-NE/HD coating

The antimicrobial peptide, DBCO-ABP, was synthesized using standard Fmoc-mediated solid phase peptide synthesis and purified to 96.02 % purity via HPLC (Fig. S5) [47]. MALDI MS analysis indicated that the monoisotopic masses of $[M+4H]^{4+}$ and $[M+3H]^{3+}$ at 654 Da and 871 Da, respectively (Fig. S6), were consistent with the theoretical molecular weight of 2612.0 Da. The successful synthesis of DBCO-ABP was also confirmed by its characteristic diagnostic peaks in the ^{1}H NMR spectrum (Fig. S7). To graft DBCO-ABP onto the optimized Cu-NE/HD coating, Azide-PEG$_4$-NHS was first covalently attached using carbodiimide chemistry, followed by DBCO-ABP grafting via click chemistry. Due to the introduction of the hydrophilic group PEG, the WCA decreased successively after grafting of the two molecules (Fig. 4A). The grafting process was quantitatively monitored using QCM-D, revealing stable binding of 80 ng cm^{-2} of Azide-PEG$_4$-NHS and a maximum grafting amount of 590 ng cm^{-2} for DBCO-ABP (Fig. 4B and C). Post-grafting chemical changes of the coating was analyzed using reflection absorbance Fourier transform infrared (RA-FTIR) spectroscopy and X-ray photoelectron spectroscopy (XPS). The Azide@Cu-NE/HD spectra displayed a characteristic peak of -N=N$^+$=N$^-$ at 2110 cm^{-1}, suggesting the effective azidation to surface by Azide-PEG$_4$-NHS (Fig. 3D). Further analysis confirmed the successful bioconjugation of DBCO-ABP, evidenced by the presence of 1,2,3-triazole groups at 1530, 1440, and 1235 cm^{-1} in the ABP@Cu-NE/HD spectrum.

Peak fitting of the C1s and N1s XPS spectra further detailed the chemical states introduced by Azide-PEG$_4$-NHS and DBCO-ABP (Fig. 4E and F). The C1s high-resolution spectrum showed an increase at 286.2 eV due to the introduction of C-O and C-N$_3$ components by Azide-PEG$_4$-NHS. After grafting DBCO-ABP, the spectrum peak increased at 284.8 eV and decreased at 286.2 eV, reflecting the introduction of C=C/C-C structures. The N1s spectrum was fitted into five peak components corresponding to various nitrogenous states, with BEs of 398.60, 399.87, 400.06, 401.28, and 404.04 eV, corresponding to C-NH$_2$, aliphatic N, azide (N=N$^-$), R-N$^+$, and azide (-N$^+$), respectively. The area ratio of [(N)-N=] to [-N$^+$] is approximately 2:1, consistent with the chemical structure of azides groups, confirming successful azidation of the Cu-NE/HD coating [48]. The disappearance of the azide peaks (-N$^+$ and ((N)-N=)) in the final coating further indicates that the DBCO-ABP was successfully grafted onto the azide-functionalized surface through the bioorthogonal N$_3$-DBCO click reaction.

Following the grafting of Azide-PEG$_4$-NHS and DBCO-ABP, the NO release rate decreased to 5.5 and 5.1 × 10^{-10} mol cm^{-2} min^{-1}, respectively (Fig. 4G and H). Stability tests revealed that after 30 days of immersion, 69 % of the NO catalytic efficiency was maintained (Fig. 4I), meeting the physiological value of 4 × 10^{-10} mol cm^{-2} min^{-1} [46].

3.2. In vitro anti-platelet and ex vivo antithrombogenic properties

Upon implantation, devices can trigger platelet adhesion and activation, initiating a blood coagulation cascade that facilitates bacterial adhesion and induces catheter-related thrombosis, potentially leading to device failure. NO, an effective mediator, attenuates platelet adhesion and activation through multiple mechanisms. It stimulates the production of cGMP by vascular endothelial cells, which directly modulates

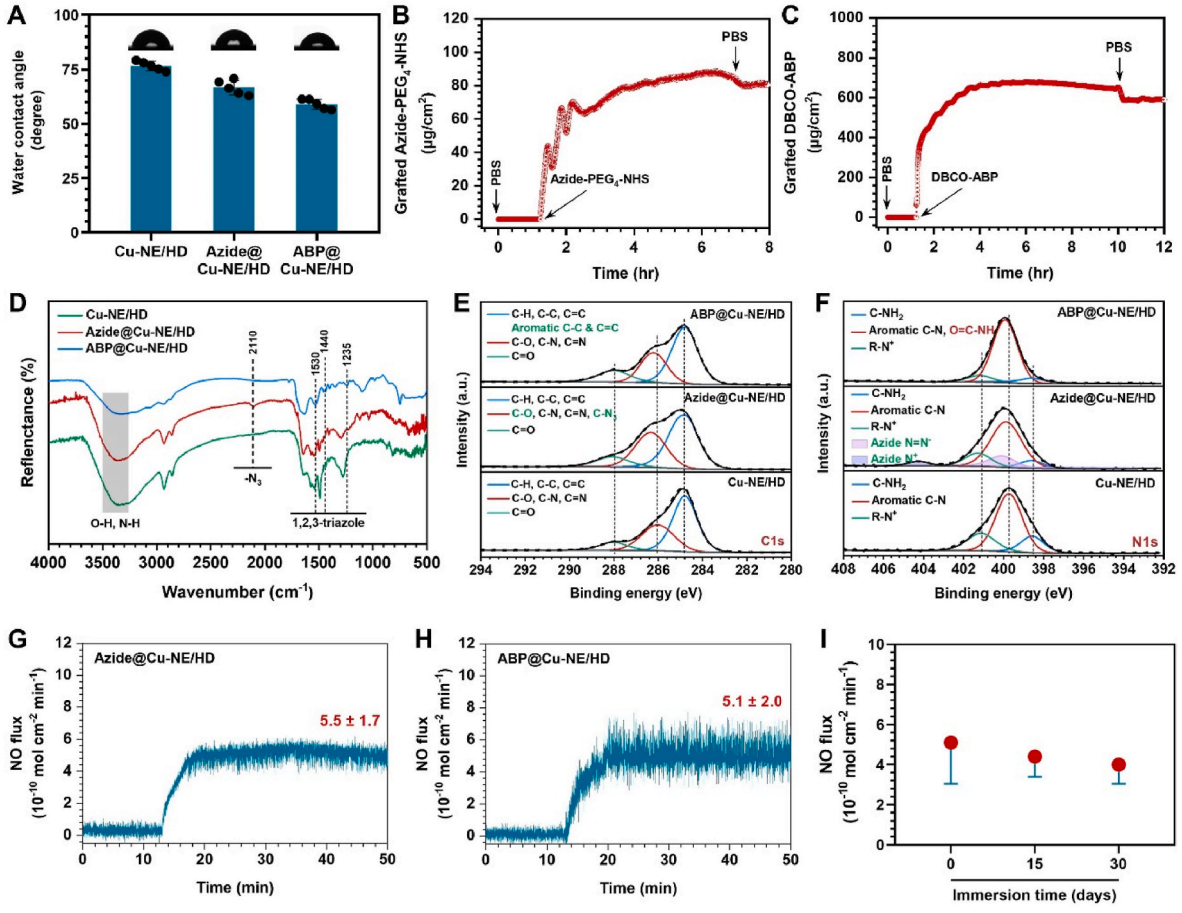

Fig. 4. (A) The WCA of the Cu-NE/HD, Azide@Cu-NE/HD and ABP@Cu-NE/HD coatings. (B, C) Real-time monitoring of Azide-PEG$_4$-NHS and DBCO-ABP molecules grafting determined by QCM-D. (D) GATR-FTIR of the Cu-NE/HD, Azide@Cu-NE/HD and ABP@Cu-NE/HD coatings. (E, F) High-resolution C1s and N1s XPS spectra of the Cu-NE/HD, Azide@Cu-NE/HD and ABP@Cu-NE/HD coatings. (G, H) NO release rates after grafting of Azide-PEG$_4$-NHS and DBCO-ABP molecules. (I) NO release rates of ABP@Cu-NE/HD-coated PVC after different immersion time. Data are presented as mean ± SD (n = 4) and analyzed by one-way ANOVA.

platelet activity. Additionally, NO binds to iron ions on the platelet membrane, inhibiting thromboxane A2 production and thus reducing platelet activation [49]. Therefore, the suppressing capacity on platelet adhesion and activation of our coating was evaluated. PRP supplemented with 10 μL NO donors (10 μM GSNO, 10 μM GSH) was incubated with the samples for 30 min. In the NO-free group (PVC, NE/HD, ABP@NE/HD), a significant number of activated platelets adhered and aggregated on the surfaces, exhibiting extensive dendritic spreading and pseudopodia formation (Fig. 5A). In contrast, the Cu-NE/HD and ABP@Cu-NE/HD groups showed reduced platelet adhesion and activation (Fig. 5B and C), indicating that NO catalyzed by Cu^{2+} effectively performs an antithrombotic function *in vitro*.

To enhance clinical relevance, we conducted *ex vivo* blood circulation experiments using rabbit arteriovenous shunt circuits (Fig. 5D). After 2 h of cardiopulmonary bypass with NO donor supplementation, all tubes were assessed for thrombus weight, occlusion rate, and blood

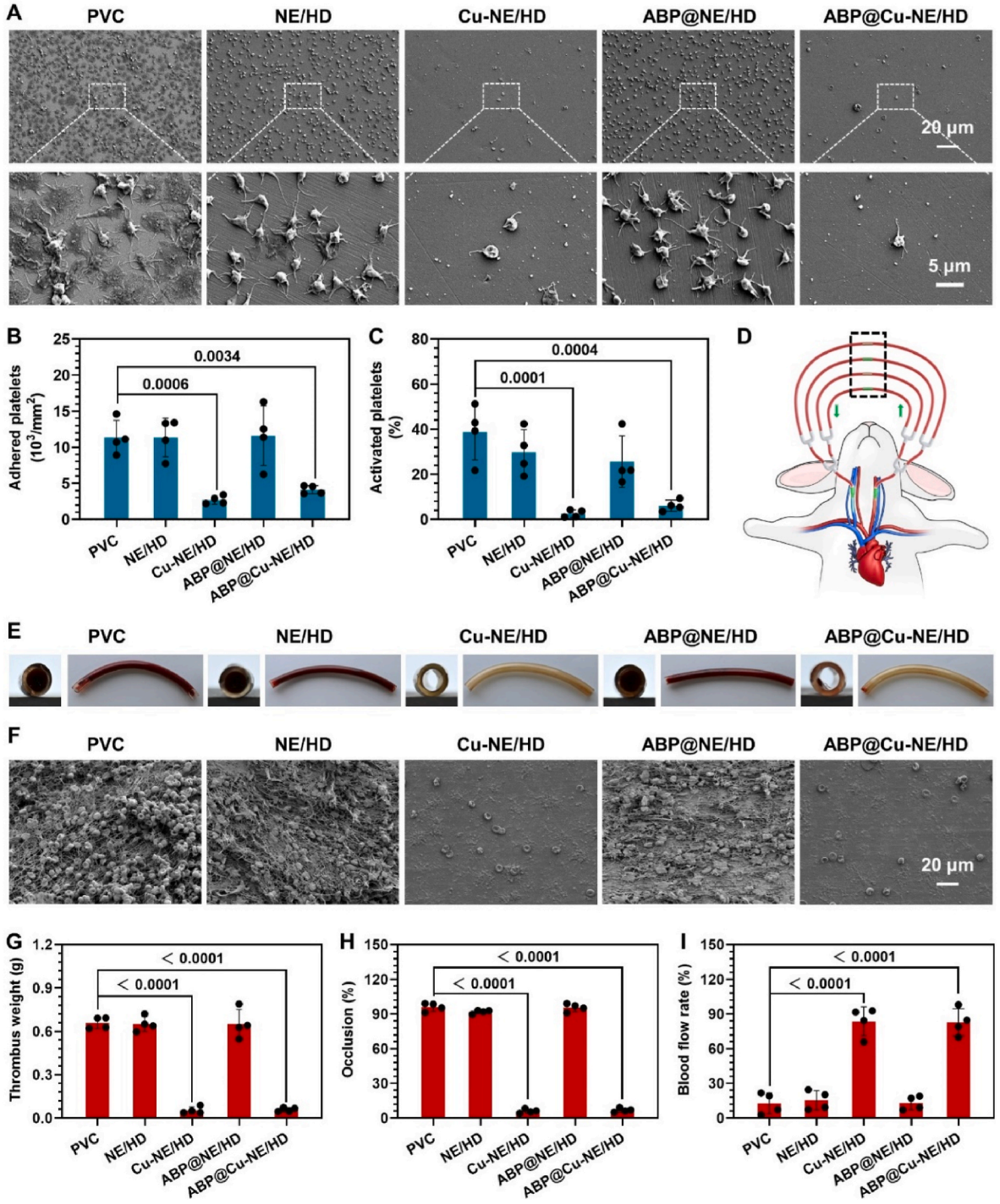

Fig. 5. (A) Representative SEM images of platelets adhered on different surfaces. Quantitative results of (B) adhesion and (C) activation of platelets incubated with uncoated-, NE/HD-, Cu-NE/HD-, ABP@NE/HD-, and ABP@Cu-NE/HD-PVC for 30 min. (D) Scheme of the New Zealand white rabbit AV shunt model exhibiting placement of the cannula in the carotid artery and jugular vein connected by different PVC tubes. (E) Photographs of different tubes and their cross sections, and (F) SEM images of the inner wall of different tubes. (G) Thrombus weight, (H) occlusion rates, and (I) blood flow rates in different tubes at the end of the circulation experiments. Data are presented as mean ± SD ($n = 4$) and analyzed using one-way ANOVA.

flow rate. Minimal thrombosis was observed in the NO release group (Cu-NE/HD and ABP@Cu-NE/HD), in contrast to severe thrombosis in the NO-free group (PVC, NE/HD, ABP@NE/HD) (Fig. 5E). SEM analysis further confirmed that the inclusion of Cu^{2+} significantly prevented thrombus formation (Fig. 5F). Extensive thrombi, along with a densely cross-linked network of fibrin, red blood cells, and activated platelets, were noted on the surfaces of bare PVC, NE/HD-coated, and ABP@NE/HD-coated tubes. Quantitative analysis revealed that the thrombus weights in the NO-free group were higher than 0.65 g. However, thrombus weights significantly decreased to 0.053 ± 0.036 g and 0.058 ± 0.014 g in the Cu-NE/HD and ABP@Cu-NE/HD groups, respectively (Fig. 5G). Additionally, occlusion rates were significantly reduced to 5.94 ± 2.34 % and 6.81 ± 2.26 % for the Cu-NE/HD and ABP@Cu-NE/HD groups, respectively, compared to near-complete blockage observed in groups without Cu^{2+} (Fig. 5H). The blood flow rate showed consistent results (Fig. 5I). Both *in vitro* studies and *ex vivo* perfusion experiments demonstrate that the NO catalyzed by Cu^{2+} in the coatings exhibits superior anti-thrombotic efficacy across various experimental conditions, unaffected by the grafted ABP molecules.

3.3. Biochemical analysis of ABP@Cu-NE/HD coating

For blood-contacting implants with prolonged indwelling time and large contact surface area, such as central venous catheters and cardiopulmonary bypass machines, systematic evaluation of their effects on the blood system, immune system, and other solid organs is necessary to ensure safety during *in vivo* use.

Considering the difference in total blood volume between rabbits and human (approximately 200 ml for adult white rabbits and approximately 4000 ml for adult human), bare PVC tubes or PVC tubes modified with ABP@Cu-NE/HD coating with an extended length of 1.6 m (inner diameter 4 mm) were applied to simulate clinical application. The tubes were placed into rabbit arteriovenous shunt circuits (Fig. 6A). Blood was collected at 0, 5, 30, and 60 min after blood circulation and used for biochemistry and measurement of physiological parameters such as inflammatory response, coagulation, and organ functions.

For both groups, the coagulation activity was unchanged after 60 min of blood contact, as evidenced by consistent levels of F_{1+2} (a biomarker of prothrombin activation) compared to the levels at time 0.

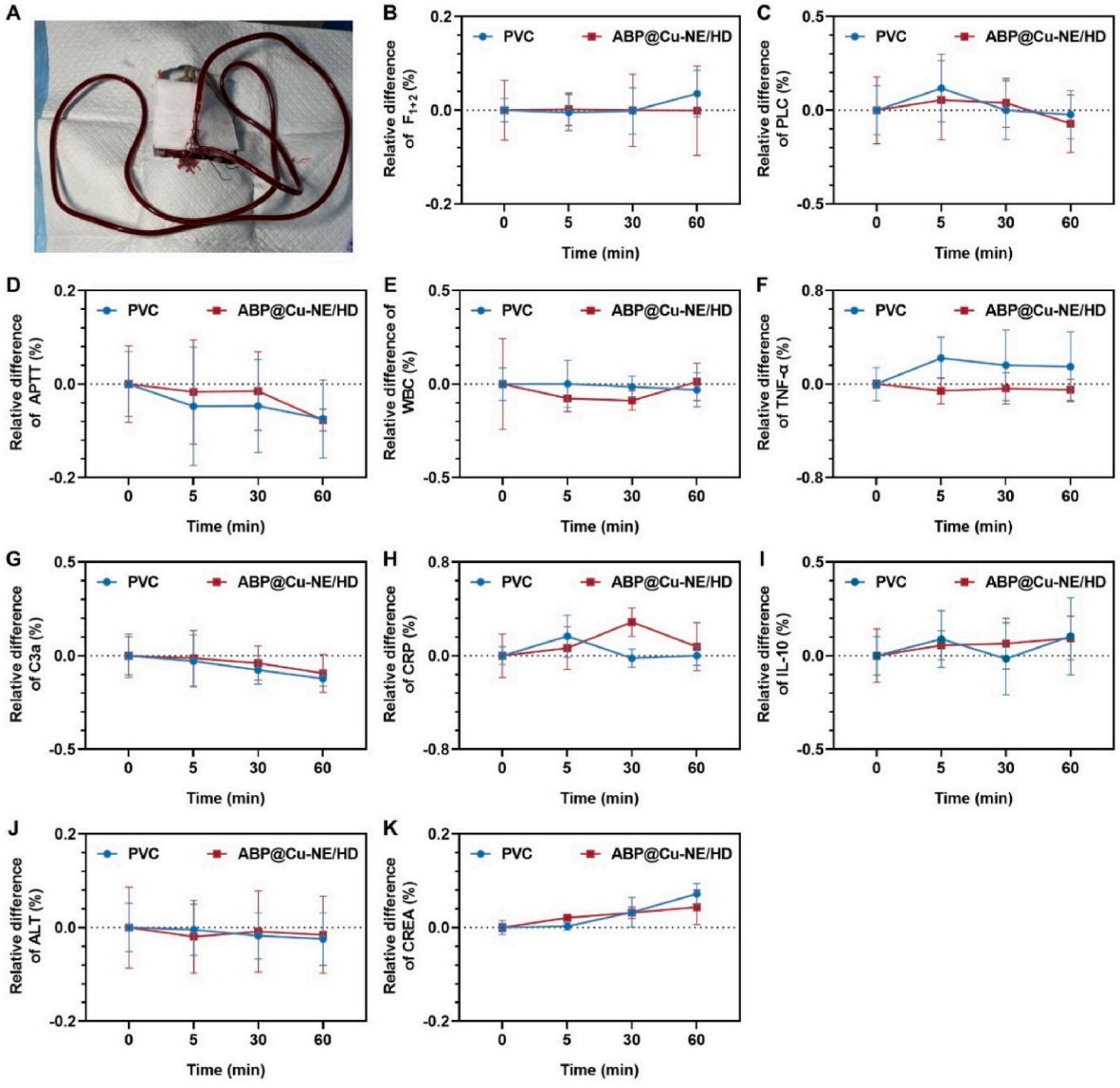

Fig. 6. (A) Circulation model on rabbit for blood analysis. Blood parameters including (B) prothrombin fragment 1 + 2 (F_{1+2}), (C) platelet count (PLC), (D) activated partial thromboplastin time (APTT), (E) white blood cells (WBC), (F) tumor necrosis factor-alpha (TNF-α), (G) Complement component 3a (C3a), (H) C-reactive protein (CRP), (I) interleukin-10 (IL-10), (J) alanine aminotransferase (ALT), and (K) creatinine (CREA). The analysis of relative difference included 0, 5, 30, and 60 min.

Moreover, neither bare PVC tubes nor those modified with ABP@Cu-NE/HD exhibited discernible impact on platelet count. However, both types of tubes demonstrated shortened APTT (a laboratory test used to assess the intrinsic pathway of coagulation and monitor anticoagulant therapy), suggesting that the external blood circulation system may influence clotting times. While NO significantly inhibited thrombus formation on the modified surfaces, it did not substantially affect the entire blood system.

After implantation, the devices were rapid recognized by the immune system, triggering an inflammatory response. Analysis of pro-inflammatory and anti-inflammatory markers such as leukocytes, TNF-α (a key pro-inflammatory cytokine involved in immune regulation and acute phase responses), C3a (a cleavage fragment of complement component C3, serving as an indicator of complement system activation and inflammation), CRP (a plasma acute phase protein utilized as a marker for inflammation and tissue damage in various clinical settings), and IL-10 (a cytokine with anti-inflammatory and immunosuppressive properties, crucial for regulating immune responses and maintaining immune homeostasis) showed consistent levels throughout the circulation process, indicating that neither the modified nor the bare PVC tubes significantly impacted the immune system.

In order to investigate the potential toxicity to organs and tissues, we measure levels of ALT (an enzyme primarily found in the liver, serving as a marker for liver function and hepatocellular injury in clinical assessments) and CREA (a commonly used marker for assessing renal function and kidney health in clinical practice). Both markers showed no significant changes, confirming the biosafety of both bare and ABP@Cu-NE/HD coated PVC groups throughout the experimental period.

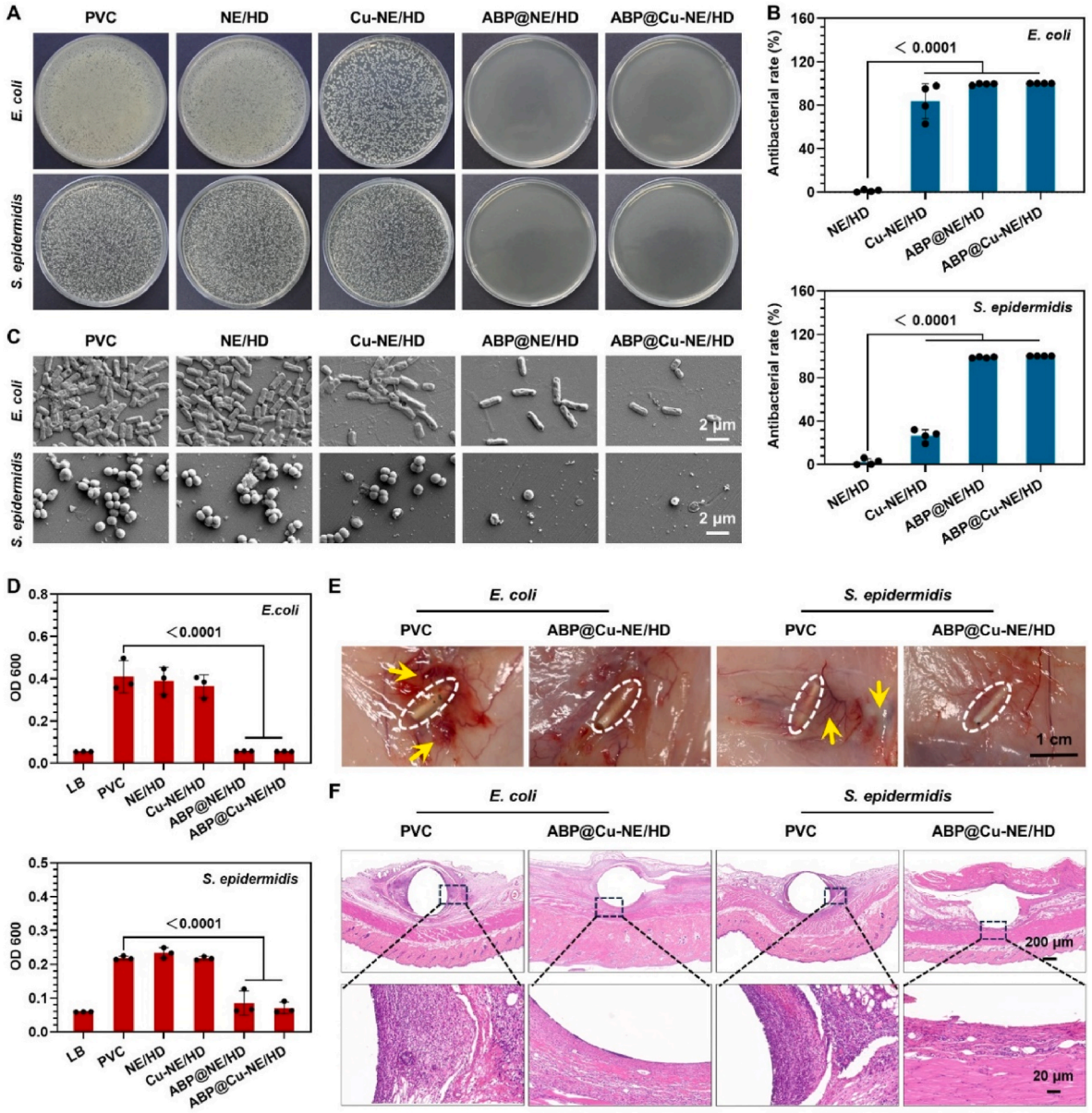

Fig. 7. (A) Representative colonization photographs of *E. coli* and *S. epidermidis* on the PVC substrates before and after functionalization with NE/HD, Cu-NE/HD, ABP@NE/HD, and ABP@Cu-NE/HD. (B) Antibacterial rate of different surfaces calculated by the results of (A). (C) SEM images of *E. coli* and *S. epidermidis* that adhered or colonized on the bare and modified PVC substrates. (D) OD 600 values of the LB broth following overnight incubation with bacteria exposed bare and modified PVC substrates. (E) The image of the inflammatory reaction in visually after establishment of rat models of the implant-associated bacterial infection in the subcutaneous implantation (5 days). (F) Histopathology micrographs of subcutaneous tissue implanted with uncoated and ABP@Cu-NE/HD-coated implants. Data are presented as mean ± SD ($n = 4$) and analyzed by one-way ANOVA.

3.4. Anti-bacterial property and in vivo anti-infection activity of the ABP@Cu-NE/HD coating

Bacterial infections post-implantation of medical devices significantly increases hospitalization duration and elevates the risk of implant failure, underscoring the necessity for antibacterial functionalization. Accordingly, we investigated the antibacterial properties of ABP-modified PVC against common post-interventional pathogens, *S. epidermidis* and *E. coli*. A droplet of bacterial suspension was placed on the samples surfaces for solid culture testing, whereas complete immersion of samples in bacterial suspensions was utilized for liquid culture. The NE/HD-modified PVC did not show antibacterial activity (Fig. 7A). Conversely, the Cu-NE/HD samples displayed noticeable antibacterial effects due to the bactericidal properties of copper ions, which were more effective against *E. coli* than *S. epidermidis* due to structural differences in their outer layers [50]. ABP-modified surfaces demonstrated effective bacterial inhibition in both solid and liquid media. Moreover, surfaces co-modified with Cu and ABP achieved nearly 100 % antibacterial efficiency (Fig. 7B).

SEM analysis revealed extensive bacterial adhesion and proliferation on uncoated and NE/HD-modified PVC, whereas ABP-functionalized surfaces significantly inhibited both adhesion and proliferation (Fig. 7C). Notably, the surfaces with Cu-NE/HD modification showed slight bacterial reduction and membrane disruption, suggesting the bactericidal impact of copper ions, although not at an ideal bacteriostatic level. However, ABP-modified surfaces exhibited bacterial membrane ruptures, highlighting the efficacy of ABP grafted through surface click chemistry in penetrating and disrupting bacterial membranes to enhance bactericidal activity. Similar results were observed in liquid media, with clear bacterial solutions in liquid media compared to the turbid solutions of control groups (Fig. 7D), confirming effective bacterial growth inhibition. In summary, the combination of ABP and Cu^{2+} in the ABP@Cu-NE/HD surfaces provides excellent antibacterial properties.

To more accurately simulate the complex *in vivo* environment, we evaluated the antibacterial performance of the modified catheter using a subcutaneous implantation model in rats. Samples contaminated with bacteria were implanted subcutaneously for 5 days. The tissue at the implantation site of the bare catheter showed significant festering and infection, whereas the site with the ABP@Cu-NE/HD-coated catheter exhibited no relevant changes (Fig. 7E). H&E staining indicated severe diffuse inflammatory infiltration around the bare catheter, contrasted by minimal inflammatory response around the ABP@Cu-NE/HD-coated catheter (Fig. 7F). This outcome confirms that the ABP@Cu-NE/HD-modified catheter not only exhibits good biocompatibility but also effectively reduces the inflammatory response by preventing bacterial infections at the implantation site.

3.5. Durability of anti-thrombotic and antibacterial properties of ABP@Cu-NE/HD coating

For clinical applications where blood-contact devices may need to remain in place from several days to weeks, the long-term efficacy of the ABP@Cu-NE/HD coating is critical. To assess this, we evaluated both the antibacterial and antithrombotic properties of the coating after extended immersion in PBS for 15 and 30 days. Our results showed that the coating maintained strong antibacterial properties throughout the testing period. Even after 30 days of immersion, it achieved an

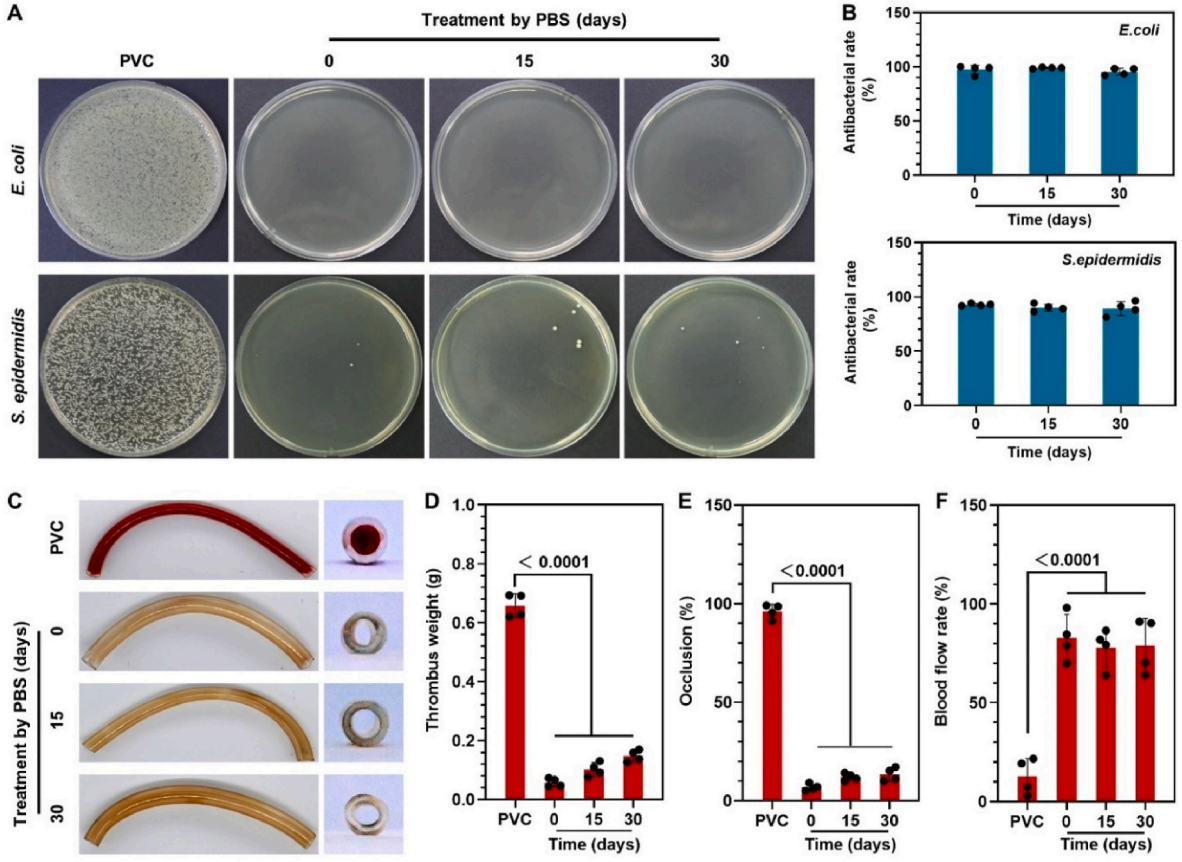

Fig. 8. (A) Colonization photographs of *E. coli* and *S. epidermidis* on bare PVC and ABP@Cu-NE/HD-coated PVC before and after treatments by PBS for different days. (B, C) Antibacterial rate of different surfaces calculated by the results of (A). (D) Photographs of different tubes and their cross sections of bare PVC and ABP@Cu-NE/HD-coated PVC tubes. (E) Thrombus weight, (F) occlusion rates, and (G) Blood flow rates in different tubes at the end of the circulation experiments. Data are presented as mean ± SD ($n = 4$) and analyzed by one-way ANOVA.

antibacterial rate exceeding 90 % against both *E. coli* and *S. epidermidis* (Fig. 8A–C). The anti-thrombotic properties were assessed using an *ex vivo* circulation test, which mimicked the blood flow conditions typical in clinical scenarios. After various durations of immersion, the bare PVC catheters showed severe thrombus accumulation (Fig. 8D). In contrast, catheters modified with the ABP@Cu-NE/HD coating retained substantial anti-thrombotic capabilities even after 30 days. This retention aligns with the continued ability of the coating to catalyze NO release after immersion. However, we observed an increase in thrombus weight and occlusion rates after 30 days compared to the initial measurements. This increase was attributed to the leakage of Cu ions, which reduced the catalytic release rate of NO from 5.1 to 4.0 $\times$ 10^{-10} mol cm^{-2} min^{-1} (Fig. S8). These findings demonstrate that the ABP@Cu-NE/HD coating retains effective antibacterial and antithrombotic properties over extended periods, confirming its potential for long-term application in implantable and interventional blood-contact devices.

4. Conclusions

In this study, we developed a biomimetic surface engineering strategy that mimics the balanced anti-thrombosis and anti-infection properties of natural vasculature on catheters. To achieve this, the therapeutic NO gas and antibacterial peptide were efficiently integrated via a stepwise metal-catechol-(amine) surface engineering strategy. Firstly, the NO catalytic substance Cu^{2+} was controllably incorporated with NE/HD network through a one-step molecular/ion self-assembly process, facilitating the precise control of NO generation behavior. Moreover, the amine groups on the Cu-NE/HD coating realized the dense grafting of ABP by the sequential immobilization of NHS-PEG_4-Azide and DBCO-ABP. The resultant coating exhibited a satisfied NO generation rate of 5.1 $\times$ 10^{-10} mol cm^{-2} min^{-1} that higher than that of healthy endothelium, and retained a releasing rate of 4.0 $\times$ 10^{-10} mol cm^{-2} min^{-1} after 30 days immersion in PBS. This durable NO release not only prevents platelet adhesion and activation but also inhibits thrombus formation in *ex vivo* circulation. Additionally, the densely grafted ABPs endows the surface with an antibacterial rate exceeding 90 % against *E. coli* and *S. epidermidis* even after 30 days of immersion. Our strategy offers an advanced solution for clinical applications aimed at addressing complications associated with thrombosis and infection in extracorporeal circuits and indwelling medical devices.

Ethics approval and consent to participate

All the animal experiments were approved by the Dongguan People's Hospital Laboratory Animal Welfare and Ethics Committee (Approval NO: IACUC-AWEC-202306111), following the guidelines of the Laboratory Animal Administration Rules of China.

Data availability statement

The data that support the findings of this study are available from the corresponding author upon reasonable request.

CRediT authorship contribution statement

Siyuan Yue: Writing – original draft, Validation, Software, Methodology, Investigation, Formal analysis, Data curation, Conceptualization. **Wentai Zhang:** Writing – review & editing, Software, Methodology, Data curation, Conceptualization. **Qing Ma:** Visualization, Software, Formal analysis. **Zhen Zhang:** Writing – review & editing, Project administration, Funding acquisition. **Jing Lu:** Data curation, Formal analysis, Methodology, Supervision, Validation, Writing – review & editing. **Zhilu Yang:** Writing – review & editing, Supervision, Project administration, Funding acquisition.

Declaration of competing interest

Prof. Zhilu Yang is an editorial board member for Bioactive Materials and was not involved in the editorial review or the decision to publish this article. All authors declare that there are no competing interests.

Acknowledgments

This work was supported by the National Natural Science Foundation of China (Project 82072072, 32261160372, 32171326, 32371377), the Guang Dong Basic and Applied Basic Research Foundation (2022B1515130010), the Natural Science Foundation of Guangdong Province (2022A1515011442), Dongguan Science and Technology of Social Development Program (20231800906311, 20221800906322).

Appendix A. Supplementary data

Supplementary data to this article can be found online at https://doi.org/10.1016/j.bioactmat.2024.09.009.

References

[1] S. Croes, E.E. Stobberingh, K.N.J. Stevens, M.L.W. Knetsch, L.H. Koole, Antimicrobial and anti-thrombogenic features combined in hydrophilic surface coatings for skin-penetrating catheters. Synergy of Co-embedded silver particles and heparin, ACS Appl. Mater. Interfaces 3 (7) (2011) 2543–2550.
[2] T. Matsuda, Device-directed therapeutic drug delivery systems, J. Contr. Release 78 (1) (2002) 125–131.
[3] E.A. Vogler, C.A. Siedlecki, Contact activation of blood-plasma coagulation, Biomaterials 30 (10) (2009) 1857–1869.
[4] I.H. Jaffer, J.I. Weitz, The blood compatibility challenge. Part 1: blood-contacting medical devices: the scope of the problem, Acta Biomater. 94 (2019) 2–10.
[5] X. Mou, H. Zhang, H. Qiu, W. Zhang, Y. Wang, K. Xiong, N. Huang, H.A. Santos, Z. Yang, Mussel-inspired and bioclickable peptide engineered surface to combat thrombosis and infection, Research 2022 (2022).
[6] W. Xiu, S. Gan, Q. Wen, Q. Qiu, S. Dai, H. Dong, Q. Li, L. Yuwen, L. Weng, Z. Teng, Y. Mou, L. Wang, Biofilm microenvironment-responsive nanotheranostics for dual-mode imaging and hypoxia-relief-enhanced photodynamic therapy of bacterial infections, Research 2020 (2020).
[7] D. Zhang, Q. Chen, C. Shi, M. Chen, K. Ma, J. Wan, R. Liu, Dealing with the foreign-body response to implanted biomaterials: strategies and applications of new materials, Adv. Funct. Mater. 31 (6) (2021) 2007226.
[8] J.W. Costerton, P.S. Stewart, E.P. Greenberg, Bacterial biofilms: a common cause of persistent infections, Science 284 (5418) (1999) 1318–1322.
[9] X. Song, H. Ji, Y. Li, Y. Xiong, L. Qiu, R. Zhong, M. Tian, J.N. Kizhakkedathu, B. Su, Q. Wei, W. Zhao, C. Zhao, Transient blood thinning during extracorporeal blood purification via the inactivation of coagulation factors by hydrogel microspheres, Nat. Biomed. Eng. 5 (10) (2021) 1143–1156.
[10] J. Peng, K. Li, Y. Du, F. Yi, L. Wu, G. Liu, A robust mixed-charge zwitterionic polyurethane coating integrated with antibacterial and anticoagulant functions for interventional blood-contacting devices, J. Mater. Chem. B 11 (33) (2023) 8020–8032.
[11] K. Liu, F. Zhang, Y. Wei, Q. Hu, Q. Luo, C. Chen, J. Wang, L. Yang, R. Luo, Y. Wang, Dressing blood-contacting materials by a stable hydrogel coating with embedded antimicrobial peptides for robust antibacterial and antithrombus properties, ACS Appl. Mater. Interfaces 13 (33) (2021) 38947–38958.
[12] R. Tian, J. Liu, G. Dou, B. Lin, J. Chen, G. Yang, P. Li, S. Liu, Y. Jin, X. Qiu, X. Chen, Synergistic antibiosis with spatiotemporal controllability based on multiple-responsive hydrogel for infectious cutaneous wound healing, Smart Materials in Medicine 3 (2022) 304–314.
[13] M. Badv, F. Bayat, J.I. Weitz, T.F. Didar, Single and multi-functional coating strategies for enhancing the biocompatibility and tissue integration of blood-contacting medical implants, Biomaterials 258 (2020) 120291.
[14] A. Kumar, H.P. Schweizer, Bacterial resistance to antibiotics: active efflux and reduced uptake, Adv. Drug Deliv. Rev. 57 (10) (2005) 1486–1513.
[15] R.E. Cronin, R.F. Reilly, Unfractionated heparin for hemodialysis: still the best option, Semin. Dial. 23 (5) (2010) 510–515.
[16] P. Prandoni, S. Siragusa, B. Girolami, F. Fabris, f.t.B.I. Group, The incidence of heparin-induced thrombocytopenia in medical patients treated with low-molecular-weight heparin: a prospective cohort study, Blood 106 (9) (2005) 3049–3054.
[17] N. Dalibon, M. Stern, P. Bonnette, G. Dreyfus, M. Fischler, Probable allergic reaction to cyclosporin and early formation of thrombi on a pulmonary artery catheter: two unusual complications during bilateral lung transplantation, Br. J. Anaesth. 89 (6) (2002) 930–933.
[18] C. Nwokolo, L. Byrne, K.J. Misch, Toxic epidermal necrolysis occurring during treatment with trimethoprim alone, Br. Med. J. 296 (6627) (1988) 970.
[19] J. Badger, Long peripheral catheters for deep arm vein venous access: a systematic review of complications, Heart Lung 48 (3) (2019) 222–225.

[20] P.J. Pronovost, C.A. Goeschel, E. Colantuoni, S. Watson, L.H. Lubomski, S. M. Berenholtz, D.A. Thompson, D.J. Sinopoli, S. Cosgrove, J.B. Sexton, J. A. Marsteller, R.C. Hyzy, R. Welsh, P. Posa, K. Schumacher, D. Needham, Sustaining reductions in catheter related bloodstream infections in Michigan intensive care units: observational study, Br. Med. J. 340 (2010) c309.
[21] D. Campoccia, L. Montanaro, C.R. Arciola, A review of the biomaterials technologies for infection-resistant surfaces, Biomaterials 34 (34) (2013) 8533–8554.
[22] H.P. Felgueiras, L.M. Wang, K.F. Ren, M.M. Querido, Q. Jin, M.A. Barbosa, J. Ji, M. C.L. Martins, Octadecyl chains immobilized onto hyaluronic acid coatings by thiol–ene "click chemistry" increase the surface antimicrobial properties and prevent platelet adhesion and activation to polyurethane, ACS Appl. Mater. Interfaces 9 (9) (2017) 7979–7989.
[23] Y. Zou, H. Zhang, Y. Zhang, Y. Wu, J. Cheng, D. Jia, C. Liu, H. Chen, Y. Zhang, Q. Yu, A near-infrared light-triggered nano-domino system for efficient biofilm eradication: activation of dispersing and killing functions by generating nitric oxide and peroxynitrite via cascade reactions, Acta Bio 170 (2023) 389–400.
[24] Y. Qu, Y. Zou, G. Wang, Y. Zhang, Q. Yu, Disruption of communication: recent advances in antibiofilm materials with anti-quorum sensing properties, ACS Appl. Mater. Interfaces 16 (11) (2024) 13353–13383.
[25] M. Yao, Z. Wei, J. Li, Z. Guo, Z. Yan, X. Sun, Q. Yu, X. Wu, C. Yu, F. Yao, S. Feng, H. Zhang, J. Li, Microgel reinforced zwitterionic hydrogel coating for blood-contacting biomedical devices, Nat. Commun. 13 (1) (2022) 5339.
[26] B. Zhang, Y. Qin, Y. Wang, A nitric oxide-eluting and REDV peptide-conjugated coating promotes vascular healing, Biomaterials 284 (2022) 121478.
[27] S.J. Peacock, T.J. Foster, B.J. Cameron, A.R. Berendt, Bacterial fibronectin-binding proteins and endothelial cell surface fibronectin mediate adherence of Staphylococcus aureus to resting human endothelial cells, Microbiology 145 (12) (1999) 3477–3486.
[28] E.J. Schiffrin, F. Rochat, H. Link-Amster, J.M. Aeschlimann, A. Donnet-Hughes, Immunomodulation of human blood cells following the ingestion of lactic acid bacteria, J. Dairy Sci. 78 (3) (1995) 491–497.
[29] G. Wang, Human antimicrobial peptides and proteins, Pharmaceuticals 7 (5) (2014) 545–594.
[30] N. Chen, C. Jiang, Antimicrobial peptides: structure, mechanism, and modification, Eur. J. Med. Chem. 255 (2023) 115377.
[31] M. Zasloff, Antimicrobial peptides of multicellular organisms: my perspective, in: K. Matsuzaki (Ed.), Antimicrobial Peptides: Basics for Clinical Application, Springer, 2019, pp. 3–6.
[32] X. Gao, J. Ding, C. Liao, J. Xu, X. Liu, W. Lu, Defensins: the natural peptide antibiotic, Adv. Drug Deliv. Rev. 179 (2021) 114008.
[33] D. Tousoulis, A.-M. Kampoli, C. Tentolouris Nikolaos Papageorgiou, C. Stefanadis, The role of nitric oxide on endothelial function, Curr. Vasc. Pharmacol. 10 (1) (2012) 4–18.
[34] Y. Wu, D. Jia, K. Lu, H. Zhang, C. Liu, Y. Lin, J. Cheng, Y. Zou, H. Xu, H. Chen, Y. Zhang, Q. Yu, Bacterial cellulose-based dressings with photothermal bactericidal activity and pro-angiogenic ability for infected wound healing, J. Mater. Sci. Technol. 160 (2023) 76–85.
[35] P. Li, W. Cai, K. Wang, L. Zhou, S. Tang, Y. Zhao, X. Li, J. Wang, Selenium-functionalized polycarbonate-polyurethane for sustained in situ generation of therapeutic gas for blood-contacting materials, Smart Materials in Medicine 3 (2022) 361–373.
[36] Y. Yang, P. Gao, J. Wang, Q. Tu, L. Bai, K. Xiong, H. Qiu, X. Zhao, M.F. Maitz, H. Wang, X. Li, Q. Zhao, Y. Xiao, N. Huang, Z. Yang, Endothelium-mimicking multifunctional coating modified cardiovascular stents via a stepwise metal-catechol-(amine) surface engineering strategy, Smart Materials in Medicine 2020 (2020).
[37] Y. Xiao, W. Wang, X. Tian, X. Tan, T. Yang, P. Gao, K. Xiong, Q. Tu, M. Wang, M. F. Maitz, N. Huang, G. Pan, Z. Yang, A versatile surface bioengineering strategy based on mussel-inspired and bioclickable peptide mimic, Smart Materials in Medicine 2020 (2020).
[38] Q. Zhang, G. Kuang, L. Wang, P. Duan, W. Sun, F. Ye, Designing bioorthogonal reactions for biomedical applications, Smart Materials in Medicine 6 (2023) 251.
[39] T. Bento de Carvalho, J.B. Barbosa, P. Teixeira, Assessing antimicrobial efficacy on plastics and other non-porous surfaces: a closer look at studies using the ISO 22196:2011 standard 13 (1) (2024) 59.
[40] Y. Xi, J. Ge, M. Wang, M. Chen, W. Niu, W. Cheng, Y. Xue, C. Lin, B. Lei, Bioactive anti-inflammatory, antibacterial, antioxidative silicon-based nanofibrous dressing enables cutaneous tumor photothermo-chemo therapy and infection-induced wound healing, ACS Nano 14 (3) (2020) 2904–2916.
[41] X. Mou, W. Miao, W. Zhang, W. Wang, Q. Ma, Z. Du, X. Li, N. Huang, Z. Yang, Zwitterionic polymers-armored amyloid-like protein surface combats thrombosis and biofouling, Bioact. Mater. 32 (2024) 37–51.
[42] J. Guo, Y. Ping, H. Ejima, K. Alt, M. Meissner, J.J. Richardson, Y. Yan, K. Peter, D. von Elverfeldt, C.E. Hagemeyer, F. Caruso, Engineering multifunctional capsules through the assembly of metal–phenolic networks, Angew. Chem. Int. Edit. 53 (22) (2014) 5546–5551.
[43] Y. Li, Y. Miao, L. Yang, Y. Zhao, K. Wu, Z. Lu, Z. Hu, J. Guo, Recent advances in the development and antimicrobial applications of metal–phenolic networks, Adv. Sci. 9 (27) (2022) 2202684.
[44] S. Hong, J. Kim, Y.S. Na, J. Park, S. Kim, K. Singha, G.I. Im, D.K. Han, W.J. Kim, H. Lee, Poly(norepinephrine): ultrasmooth material-independent surface chemistry and nanodepot for nitric oxide, Angew. Chem. Int. Ed. Engl. 52 (35) (2013) 9187–9191.
[45] Q. Tu, X. Shen, Y. Liu, Q. Zhang, X. Zhao, M.F. Maitz, T. Liu, H. Qiu, J. Wang, N. Huang, Z. Yang, A facile metal–phenolic–amine strategy for dual-functionalization of blood-contacting devices with antibacterial and anticoagulant properties, Mater. Chem. Front. 3 (2) (2019) 265–275.
[46] J. MacMicking, Q.-w. Xie, C. Nathan, Nitric oxide and macrophage function, Annu. Rev. Immunol. 15 (1) (1997) 323–350.
[47] Z. Yang, X. Zhao, R. Hao, Q. Tu, X. Tian, Y. Xiao, K. Xiong, M. Wang, Y. Feng, N. Huang, G. Pan, Bioclickable and mussel adhesive peptide mimics for engineering vascular stent surfaces, Proc. Natl. Acad. Sci. U. S. A 117 (28) (2020) 16127–16137.
[48] V.V. Rostovtsev, L.G. Green, V.V. Fokin, K.B. Sharpless, A stepwise huisgen cycloaddition process: copper(I)-Catalyzed regioselective "ligation" of azides and terminal alkynes, Angew. Chem. 33 (43) (2002) 45, 45.
[49] B.L. Nguyen, M. Saitoh, J.A. Ware, Interaction of nitric oxide and cGMP with signal transduction in activated platelets, AM. J. Physiol-Heart C. 261 (4) (1991) H1043–H1052.
[50] O. Metryka, D. Wasilkowski, A. Mrozik, Insight into the antibacterial activity of selected metal nanoparticles and alterations within the antioxidant defence system in Escherichia coli, Bacillus cereus and Staphylococcus epidermidis, Proc. Natl. Acad. Sci. U. S. A. 22 (21) (2021) 11811.